Journal of Porphyrins and Phthalocyanines
J. Porphyrins Phthalocyanines 2019; **23**: 841–849
DOI: 10.1142/S1088424619500925

Published at http://www.worldscinet.com/jpp/

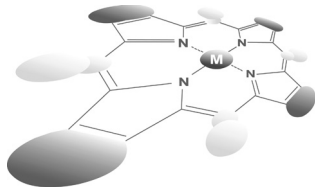

Photophysical properties of porphyrinic covalent cages endowed with different flexible linkers

Daniel Sánchez-Resa[a], Laetitia Schoepff[b], Ryan Djemili[b], Stéphanie Durot[b], Valérie Heitz*[b] and Barbara Ventura*[a]

[a] *Istituto ISOF-CNR, Via P. Gobetti 101, 40129 Bologna, Italy*
[b] *Laboratoire de Synthèse des Assemblages Moléculaires Multifonctionnels, Institut de Chimie de Strasbourg, CNRS/UMR 7177, Université de Strasbourg, 4, Rue Blaise Pascal, 67000 Strasbourg, France*

This paper is part of the 2019 Women in Porphyrin Science special issue.

Dedicated to Dr. Lucia Flamigni, an excellent scientist and a mentor in the photophysics of porphyrin assemblies.

Received 31 May 2019
Accepted 12 July 2019

ABSTRACT: In-depth photophysical studies of four flexible covalent cages bearing either two free-base porphyrins or one free-base porphyrin and one Zn(II) porphyrin, connected by linkers of different lengths, are reported. In the case of the cages with two free-base porphyrins, exciton coupling between the porphyrins is evidenced by large and split Soret bands in the absorption spectra, but the different length of the linkers has only a slight effect on their emission properties. Strong electronic interactions between the porphyrins are also evidenced for the cages that incorporate a free-base porphyrin and a Zn(II) porphyrin, with a more pronounced splitting of the Soret band for the system with longer linkers. In these cages, following excitation of the Zn-porphyrin component, an almost quantitative energy transfer to the free-base unit occurs, with a rate 1.4 times faster in the cage with longer linkers (1.4×10^{11} s^{-1} *vs.* 1.0×10^{11} s^{-1}). This difference might reflect the more flattened conformation adopted by the cage equipped with longer and more flexible linkers, the latter allowing for a shorter interplanar distance between the porphyrins. The results are discussed in terms of classical and short-range energy transfer mechanisms.

KEYWORDS: porphyrins, molecular cages, photoinduced energy transfer.

INTRODUCTION

The design of functional systems based on molecular capsules has shown great potential in nanochemistry, since these systems can work as nanoreactors, molecular recognition systems or drug carriers, providing a confined environment that enhances molecular reactivity and catalysis [1–3].

Among the different possibilities in the design of molecular cages, the choice of metallated or free-base porphyrins leads to attractive architectures due to their chemical stability and their mimicry of natural chromophores [1, 4–20]. Indeed, conversion of light energy into chemical energy performed in photosynthesis relies on efficient multistep energy transfer processes between natural chromophores belonging to the family of porphyrin derivatives (chlorophyll or bacteriochlorophyll molecules) organized in antennas that convey the energy towards the reaction center where the first electron transfer step towards a free-base porphyrin derivative occurs [21–27]. The efficiency of such processes is determined by the distance and mutual arrangement of these chromophores, and light-responsive cages have gained interest due to their ability to perform and control energy transfer processes [6, 7, 18, 28].

We have shown that bis-Zn(II) porphyrin cages equipped with four flexible linkers incorporating

*Correspondence to: Valérie Heitz, tel.: 33 (0)3 68 85 13 57, email: v.heitz@unistra.fr, Barbara Ventura, tel.: 0039 051 6399817, email: barbara.ventura@isof.cnr.it.

peripheral 1,2,3-triazole binding sites allow for a control of the distance and orientation between the two zinc(II) porphyrins. The cages adopt, in solution and in the solid state, a flattened conformation based on π–π interactions between the porphyrins, whereas a large conformational change occurs in solution upon binding four Ag(I) ions to the peripheral ligands, leading to open cages with two cofacial porphyrins separated by about 9 Å [29–32]. Based on their tunable cavity size, these cages were evaluated as switchable receptors and their capacity to behave as allosteric receptors towards different kinds of guest molecules (a coordinating or a π-acceptor molecule) was demonstrated [31].

We here report on bis-porphyrin cages constituted by either two free-base porphyrins or one zinc(II) porphyrin and one free-base porphyrin, connected by four flexible connectors that incorporate two 1,2,3-triazole ligands linked with either an ethyleneglycol unit or a diethyleneglycol unit. The latter units confer different lengths to the connectors, leading to different possible conformations of the systems. The four cages thus differ both in terms of porphyrin composition and lengths of the linkers. The study of the photophysical properties of these porphyrin cages is of importance regarding their potential as optical sensors of guest inclusion [33, 34]. Therefore, a detailed photophysical investigation has been performed by means of steady-state and time-resolved absorption and emission spectroscopy. The absorption and emission features of the cages and the photoinduced processes occurring within the porphyrin components are discussed in relation to the porphyrin nature and the structural difference between the systems.

RESULTS AND DISCUSSION

Synthesis and characterization

The synthesis of the cages incorporating two free-base or two zinc(II) porphyrins connected with short linkers [30] and with long linkers [29] have previously been reported as well as the model compounds **2H-alkyne** and **Zn-alkyne** [32] (Chart S1).

Both Zn(II)-monometallated cages, **Zn-S-2H** and **Zn-L-2H,** were prepared from cages incorporating two free-base porphyrins following a related procedure (Scheme 1). They were reacted with 1.1 equiv of $Zn(OAc)_2 \cdot 2H_2O$ in a mixture of $CHCl_3$/MeOH or CH_2Cl_2/MeOH [29, 30]. From the mixture of three cages (Zn(II)-monometallated cage, Zn(II) dimetallated cage and bis(free-base porphyrin) cage) thus obtained, the Zn(II)-monometallated cages **Zn-S-2H** and **Zn-L-2H** were isolated in 31% and 26% yield respectively, by preparative silica thin layer chromatography. They were characterized by 1D and 2D (COSY, NOESY) NMR experiments and mass spectrometry (see Figs S1–S13).

Photophysical characterization

Absorption and emission features of the four cages were characterized in DCM : MeOH (90:10). Model compounds **2H-alkyne** and **Zn-alkyne** were also studied for comparison purposes.

Cages **2H-S-2H** and **2H-L-2H**, composed by two identical free-base porphyrins, show similar absorption spectra, with a Soret band which is slightly split and broadened compared with the sum of two spectra of the monomeric model **2H-alkyne** (Fig. 1; see Fig. S14 for the spectrum of the model). These features can be ascribed to exciton coupling within the porphyrin units which are placed in close proximity in the cages, as previously observed and discussed for corresponding dimetallated Zn(II) cages [32]. The different lengths of the linkers slightly affect the absorption properties of the two cages. Indeed, the integrated molar absorption coefficients are almost identical for the two cages (1.18×10^9 $M^{-1} \cdot cm^{-2}$ and 1.17×10^9 $M^{-1} \cdot cm^{-2}$ for **2H-S-2H** and **2H-L-2H**, respectively) and close to twice the absorption coefficient of the monomer **2H-alkyne** (4.02×10^8 $M^{-1} \cdot cm^{-2}$).

The absorption spectra of the Zn(II)-monometallated cages **Zn-S-2H** and **Zn-L-2H** are shown in Fig. 2 and compared with the sum of the absorption spectra of models **2H-alkyne** and **Zn-alkyne**. The Soret bands of the cages testify to inter-porphyrinic interactions, with a more pronounced exciton splitting in the cage with longer linkers, **Zn-L-2H**. The observed features

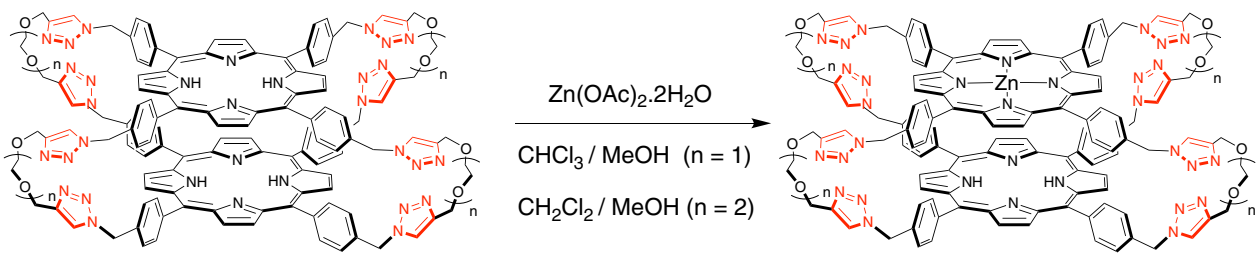

Scheme 1. Synthesis of the Zn(II)-monometallated porphyrin cages **Zn-S-2H** and **Z-L-2H**

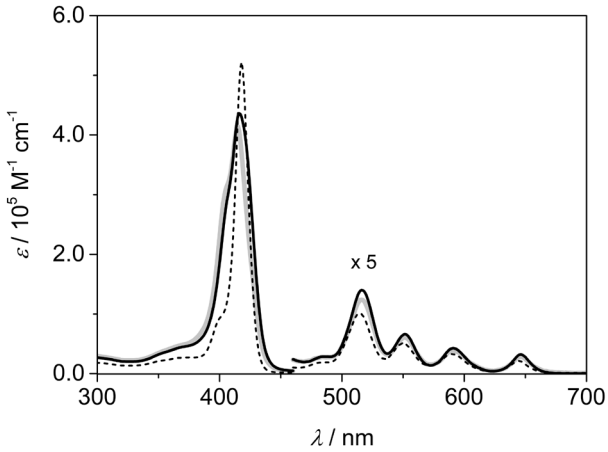

Fig. 1. Absorption spectra of **2H-S-2H** (gray), **2H-L-2H** (black full) and twice the absorption spectrum of **2H-alkyne** (black dashed) in DCM:MeOH (90:10). Absorption in the 460–700 nm region is amplified by a factor of five

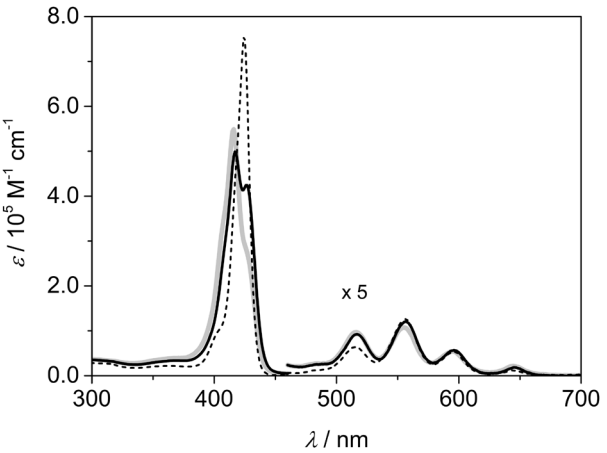

Fig. 2. Absorption spectra of **Zn-S-2H** (gray), **Zn-L-2H** (black full) and the sum of the absorption spectra of **2H-alkyne** and **Zn-alkyne** (black dashed) in DCM:MeOH (90:10). Absorption in the 460–700 nm region is amplified by a factor of five

are in accordance with a more slipped displacement of the porphyrins in **Zn-L-2H** with respect to a cofacial disposition favored in the cage with shorter and more rigid linkers, **Zn-S-2H**, a structural description provided by theoretical modelling performed on our bis Zn-porphyrin cages analogs [32]. As a confirmation, integrated molar absorption coefficients of 1.32×10^9 $M^{-1} \cdot cm^{-2}$ and 1.29×10^9 $M^{-1} \cdot cm^{-2}$ are calculated for **Zn-S-2H** and **Zn-L-2H**, respectively, values very close to the sum of the coefficients for **2H-alkyne** and **Zn-alkyne** (1.06×10^9 $M^{-1} \cdot cm^{-2}$). To better take into account the coupling interactions, the spectra of the monometallated cages have been compared with the sum of half the spectra of the parent cages containing two identical porphyrins, *i.e.* the bis free-base **2H-S-2H** and **2H-L-2H** studied here and the two dimetallated Zn(II) cages **Zn-S-Zn** and **Zn-L-Zn** previously reported [32]. The comparison for **Zn-S-2H** and **Zn-L-2H** with the sum of the respective free-base and Zn "half cages" is shown in Fig. S15. It is evident that in both cases the sum overlaps with a good approximation to the experimental spectrum of the monometallated cage, even in the Soret region which is more affected by inter-porphyrinic exciton coupling. It derives that the cages with two free-base or two Zn-porphyrins can be considered, from the photophysical point of view, as better models for the monometallated cages than the monomeric units **2H-alkyne** and **Zn-alkyne**, due to the strong interactions experienced by the porphyrins within these cages.

Luminescence determinations were performed both at room temperature in DCM:MeOH (90:10) and at 77K in a frozen DCM:MeOH (50:50) matrix.

Cages **2H-S-2H**, **2H-L-2H** show similar emission features than the model **2H-alkyne**, with maxima at *ca.* 652 nm and 718 nm, fluorescence quantum yields close to 0.080 and excited state lifetimes on the order of 9.0 ns at room temperature (Fig. 3 and Table 1), indicating that the emission properties of the free-base porphyrin components are not affected by the conformation of the cages. On the other hand, selective excitation of the free-base unit at 630 nm in **Zn-S-2H** and **Zn-L-2H** (see Fig. S15) results in a lower quantum yield of 0.047 and 0.068, respectively (Table 1), which is paralleled by a reduced lifetime of 6.7 ns and 7.6 ns. This reveals a significant perturbation of the emission properties of the free-base component in the monometallated cages due to the presence of the Zn-porphyrin counterpart. A possible explanation is the close proximity of the Zn center of the metallated porphyrin to the core of the free-base partner, which can lead to a change in molecular symmetry or to an increased intersystem crossing rate [35–37] in the latter.

In order to confirm that the perturbation of the fluorescence features of the free-base porphyrin are due

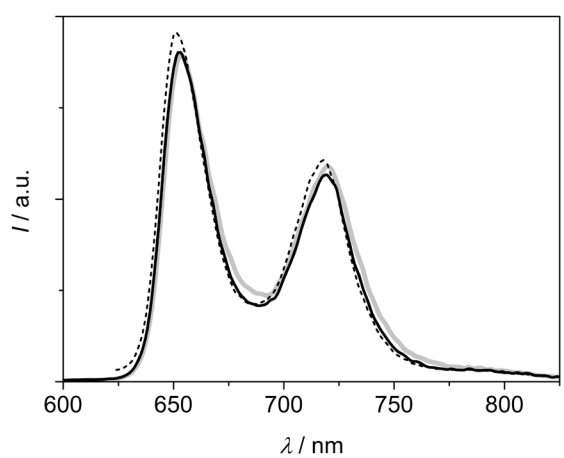

Fig. 3. Corrected emission spectra at room temperature of **2H-S-2H** (gray), **2H-L-2H** (black full) and **2H-alkyne** (black dashed) in DCM:MeOH (90:10). The spectral areas are proportional to the emission quantum yields. $\lambda_{exc} = 550$ nm

Table 1. Luminescence data at room temperature and 77K, in DCM:MeOH (90:10) and (50:50), respectively

		RT			77 K		
		λ_{max}/nm[a]	ϕ_{fl}[b]	τ/ns[c]	λ_{max}/nm[a]	τ/ns[c]	*E*/eV
2H-alkyne	^{1}2H	652, 718	0.083	8.5	648, 716	11.4	1.91
Zn-alkyne[f]	^{1}Zn	606, 658	0.040	1.7	599, 656	2.1	2.07
	^{3}Zn				782	19.2×10^6	1.59
2H-S-2H	^{1}2H-2H	654, 720	0.078	9.0	648, 716	12.8	1.91
2H-L-2H	^{1}2H-2H	652, 719	0.082	9.0	647, 715	11.5	1.92
Zn-S-2H	Zn-^{1}2H	652, 717	0.047[d]	6.7	645, 713	11.5	1.92
	^{1}Zn-2H	606, —	—	0.010[e]	601, —	—	2.06
	^{3}Zn-2H				788	15.0×10^6	1.57
Zn-L-2H	Zn-^{1}2H	652, 718	0.068[d]	7.6	644, 712	11.2	1.93
	^{1}Zn-2H	608, —	—	0.007[e]	602, —	—	2.06
	^{3}Zn-2H				787	17.9×10^6	1.58

[a]From corrected emission spectra. [b]Fluorescence quantum yields, measured with reference to TPP (*meso* tetraphenylporphyrin) in aerated toluene as a standard. [c]Fluorescence and phosphorescence lifetimes, excitation at 465 nm and 420 nm, respectively. [d]Upon selective excitation of the free-base component at 630 nm. [e]Fluorescence lifetimes measured with a streak camera apparatus (time resolution: 1 ps), excitation at 560 nm. [f]From Ref. [32].

to the close proximity of the Zn-porphyrin component in the monometallated cages, an equimolar mixture of the models **2H-alkyne** and **Zn-alkyne** has been analyzed. Figure S16 reports absorption and emission spectra of the mixture, compared with the sum of the spectra of the single compounds. The emission spectrum of the mixture is in good agreement with the sum of the spectra of the models (Fig. S16b), indicating that there is no interaction between them in solution.[§] Moreover, a lifetime of 8.6 ns has been measured for the emission of **2H-alkyne** at 720 nm in the mixture, identical to that of the model alone (Table 1).

Upon excitation of both Zn- and free-base porphyrin components in the monometallated cages, the resulting luminescence is dominated by the bands of the free-base unit, while the Zn-porphyrin emission only appears as a weak band at *ca.* 608 nm (Table 1 and Fig. 4). To estimate the extent of the quenching of the Zn-porphyrin component in these cages, the emission of **Zn-S-2H** and **Zn-L-2H** has been compared to that of optically matched solutions of model cages with two free-base units or two Zn-porphyrins, and the results are shown in Fig. 4. The excitation wavelengths were selected according to the absorption comparison previously described (Fig. S15), aiming at a substantial excitation of the Zn-porphyrin component in the monometallated cages (from 60% to 80% of the absorbed photons). By taking into account the portion of absorption of the Zn-porphyrin unit in each cage in solution and comparing the intensity of the residual Zn-porphyrin emission at 608 nm with the intensity at the same wavelength for the bis Zn-porphyrin model, it derives that the Zn-porphyrins components are quenched over 90% in **Zn-S-2H** and **Zn-L-2H**. This very efficient quenching can be safely ascribed to an energy transfer process to the free-base porphyrin counterpart. In fact, it is accompanied by a full recovery of the free-base porphyrin emission (Fig. 4): the bands at 652 and 718 nm recover for *ca.* 65% and 80% those of the bis free-base porphyrin model for **2H-S-2H** and **Zn-S-Zn**, respectively, mirroring the ratios between the quantum yield of the free-base porphyrin unit in the monometallated cages and that of the same unit in the models (Table 1). A further confirmation of an almost complete Zn→2H energy transfer process comes from the good superimposition of excitation spectra, collected for both **Zn-S-2H** and **Zn-L-2H** at 720 nm where only

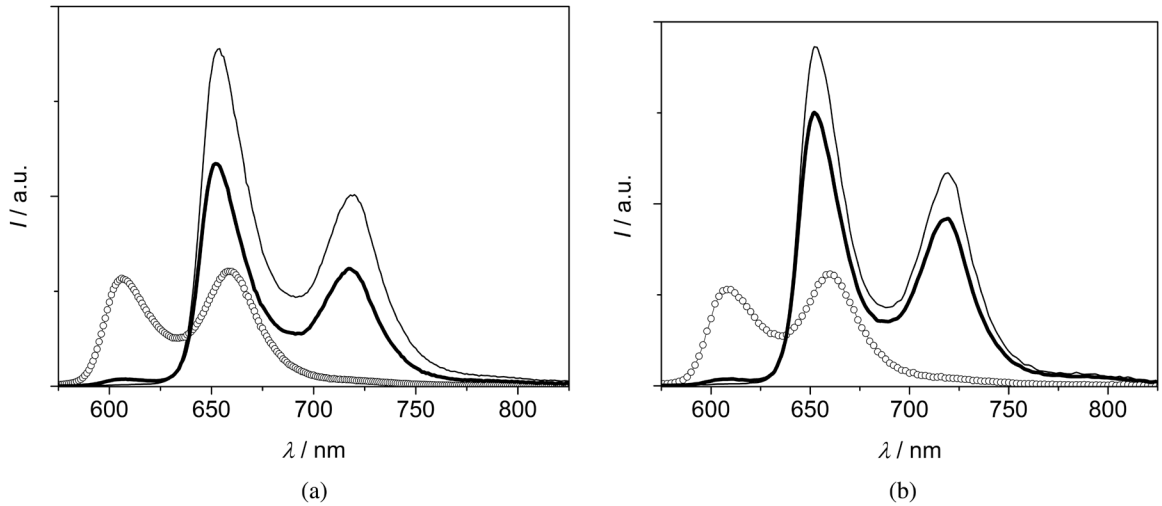

Fig. 4. Corrected emission spectra at room temperature of iso-absorbing solutions of (a) **Zn-S-2H** (black thick) and models **2H-S-2H** (black thin) and **Zn-S-Zn** (dots), excitation at 557 nm (80% of the photons absorbed by the Zn unit in **Zn-S-2H**), A_{557} = 0.067; (b) **Zn-L-2H** (black thick) and models **2H-L-2H** (black thin) and **Zn-L-Zn** (dots), excitation at 537 nm (60% of the photons absorbed by the Zn unit in **Zn-L-2H**), A_{537} = 0.046; in DCM:MeOH (90:10)

the free-base porphyrin unit emits, and absorption spectra (Fig. S17), indicating that whatever is the excited unit, the energy is conveyed to the lowest singlet excited state of the free-base porphyrin component.

As a verification that the observed energy transfer process is not occurring in freely diffusing porphyrin monomers, an equimolar mixture of models **2H-alkyne** and **Zn-alkyne**, excited at 557 nm, displays an emission spectrum perfectly matching with the sum of the spectra of the models (Fig. S18b), evidencing that there is no quenching of the Zn-porphyrin bands. Moreover, a fluorescence lifetime of 1.7 ns is measured for the mixture at 610 nm, coincident with that of **Zn-alkyne** (Table 1).

Emission measurements at 77K in a DCM:MeOH (50:50) glassy mixture allowed definition of singlet excited state energy levels for all porphyrin components of the four cages and triplet excited state levels for the Zn-porphyrins in the monometallic cages, where phosphorescence was observed in gated mode. Luminescence spectra are shown in Figs S19 and S20 and the relevant data are summarized in Table 1. It can be noticed that, in the monometallated cages, the Zn-porphyrin fluorescence is suppressed similarly to the room temperature case (Fig. S20), indicating that the quenching process occurring within these cages is very efficient even at low temperature.

In order to better characterize the photoinduced events, time-resolved luminescence experiments in the picosecond range were conducted for **Zn-S-2H** and **Zn-L-2H**. The measurements have been performed upon excitation at 560 nm, where the Zn-porphyrin component is prevalently excited, with a 100 fs pulsed laser and acquiring luminescence images with a streak camera apparatus (time resolution: 1 ps). Low laser power

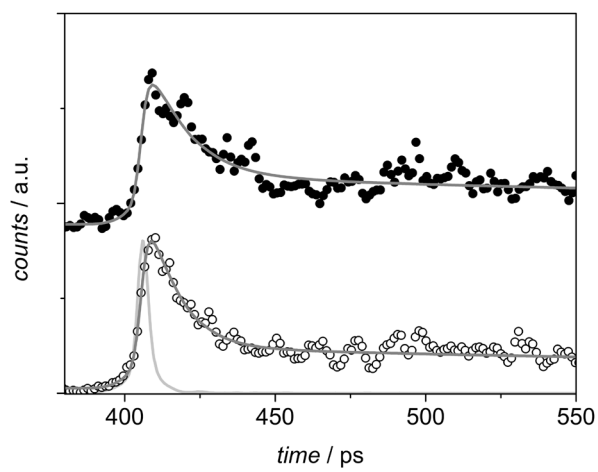

Fig 5. Normalized luminescence decays in the 600–620 nm spectral region for **Zn-S-2H** (full dots) and **Zn-L-2H** (open dots). The bi-exponential fittings are reported as grey lines. The excitation profile is shown in light grey. Excitation at 560 nm (26 μJ/pulse)

and fast image acquisition in analog integration mode were used (see the Experimental section for details) to prevent photo-degradation of the compounds. The images identify the existence of a fast process, where a decay in the emission region of the Zn-porphyrin (600–620 nm) is accompanied by a rise in the 700–750 nm spectral region, where only emission from the free-base component is observable (Fig. 5 and Fig. S21). The decay of the Zn-porphyrin luminescence can be fitted with a bi-exponential function where the main component has a lifetime of 10 ps in **Zn-S-2H** and 7 ps in **Zn-L-2H** (Fig. 5). The longer component (accounting for *ca.* 10%

of the decay) can be attributed to a tail of the free-base porphyrin emission or a minor presence of a photoproduct. A precise fitting of the rise time of the free-base signal is difficult, but is compatible with the lifetime of the quenched Zn-porphyrin emission (Fig. S21), confirming the sensitization of the free-base singlet excited state upon energy transfer from the Zn-porphyrin component.

The difference between the quenched lifetimes of the Zn-porphyrin component in the two cages is minimal but significant and indicates that the energy transfer process is faster in **Zn-L-2H** than in **Zn-S-2H**. The energy-transfer rate, in fact, is $(1.0 \pm 0.1) \times 10^{11}$ s^{-1} and $(1.4 \pm 0.2) \times 10^{11}$ s^{-1} for **Zn-S-2H** and **Zn-L-2H**, respectively (see the Experimental section for details). It derives that the process occurs with an efficiency close to 100% in both cages. To better analyze the nature of the energy transfer process, the data have been treated according to the Förster-type mechanism, which is usual between porphyrin chromophores. The overlap integral (J^F) between the emission spectrum of the donor (the bis Zn-porphyrin model) and the absorption spectrum of the acceptor (half the absorption spectrum of the bis free-base porphyrin cage) has been calculated to be 1.96×10^{-14} $cm^3 \cdot M^{-1}$ and 1.88×10^{-14} $cm^3 \cdot M^{-1}$ for **Zn-S-2H** and **Zn-L-2H**, respectively. An estimation of the geometrical factor K^2 (see the Experimental section) gives values of 0.09 for the cage with short linkers and 1.88 for the cage with long linkers (by considering $\theta_D = \theta_A = 40° \div 90°$ in **Zn-S-2H** and $\theta_D = \theta_A = 15° \div 40°$ in **Zn-L-2H** and ϕ varying from 0° and 60°, according to the geometrical parameters derived for similar cages) [32]. With these parameters, and taking into account the fluorescence quantum yield and the lifetime of the donor in both cases, it is possible to evaluate the donor–acceptor distances that should result in the experimental rate constants on the basis of a Förster-type energy-transfer mechanism. The obtained distances are 6.6 Å and 11.0 Å for **Zn-S-2H** and **Zn-L-2H**, respectively. While the first value is in good agreement with the distance between the two porphyrins estimated in the parent system (7 Å), the second value is not reasonable for a system where the long linkers allow for a closer interaction between the porphyrins. Although the estimation of K^2 for these systems involves approximations, in the case of **Zn-L-2H** a possible deviation from the classical Förster treatment can be envisaged, with a weaker short-range dependence of the rate constant, as already observed for closely spaced π systems [38]. At a supposed interplanar distance of 4 Å, estimated for the parent cage [32], we cannot also exclude a contribution from an electron exchange (Dexter) mechanism, that has been found to be operative at very short (<5–6 Å) donor–acceptor distances in cofacial porphyrinic systems [39, 40]. More detailed investigations on the nature of the energy-transfer process are under way.

EXPERIMENTAL

General

All chemicals were of the best commercially available grade and used without further purification. CH_2Cl_2 and $CHCl_3$ were distilled over CaH_2 before use. Column chromatography was carried out using silica gel (Merck, silica gel 60, 63–200 or 40–63 μm). Mass spectra were obtained by using a Bruker MicroTOF spectrometer in electrospray mode (ES-MS). Nuclear Magnetic Resonance (NMR) spectra for ^1H and ^{13}C were acquired on Bruker AVANCE 300, 400, 500 spectrometers. The ^1H and ^{13}C spectra were referenced to residual solvent peaks. ($CDCl_3$, 7.24 and 77.16; CD_2Cl_2, 5.32 and 53.84; DMSO, 2.50 and 39.52; DMF, 8.03 and 163.15).

Synthesis

Synthesis of monometallated cage Zn-S-2H. Zinc acetate $Zn(OAc)_2.2H_2O$ (5.4 mg, 24.8 μmol, 1.1 equiv.) was added to a stirred solution of cage **2H-S-2H** (50.0 mg, 22.5 μmol, 1 equiv.) in 25 mL $CHCl_3$/MeOH (9:1 v/v) at room temperature. Completion was checked by thin layer chromatography (SiO_2, CH_2Cl_2/$CHCl_3$/MeOH 5/5/1). After three hours, the solvent was evaporated and the residue was purified by two consecutive preparative thin layer chromatographies eluted with CH_2Cl_2/$CHCl_3$/MeOH 45/45/10 and flash chromatography using CH_2Cl_2/MeOH 95/5) to afford a purple solid (16 mg, 31% yield). **^{1}H NMR** (500 MHz, DMF-d_7): δ (ppm) = 8.49 (8 H, br s, $H_{pyr'}$), 8.42 (8 H, s, H_{pyr}), 8.37 (8 H, s, H_t, $H_{t'}$), 8.12 (4 H, d, ^3J = 7.6 Hz, $H_{o' out}$), 8.08 (4 H, d, ^3J = 7.6 Hz, $H_{o\ out}$), 7.79 (4 H, d, ^3J = 7.6 Hz, $H_{m' out}$), 7.74 (4 H, d, ^3J = 7.6 Hz, $H_{m' out}$), 7.14 (4 H, d, ^3J = 7.6 Hz, $H_{o' in}$), 7.09 (4 H, d, ^3J = 7.6 Hz, $H_{o\ in}$), 6.72 (8 H, m, ^3J = 7.6 Hz, $H_{m\ in}$, $H_{m' in}$), 5.84 (8 H, s, $H_{1'}$), 5.81 (8 H, s, H_1), 4.70 (16 H, s, H_2, $H_{2'}$), 3.76 (16H, m, H_3), -3.19 (2 H, s, NH). **^{13}C NMR** (126 MHz, DMF-d_7): δ (ppm) = 150.5 (C_2), 146.2 ($C_{10+10'}$), 143.6 (C_4), 142.0 ($C_{4'}$), 137.0 ($C_{5' out}$), 136.3 ($C_{5\ out}$), 135.7–135.4 C_7 + $C_{7'}$ + $C_{5' in+5 in}$), 132.4 (C_1), 127.5 ($C_{6' out}$), 127.2 ($C_{6\ out}$), 126.7 ($C_{6' in}$), 126.3 ($C_{6\ in}$), 125.4 ($C_{9'}$), 125.3 (C_9), 120.8 (C_3), 120.6 ($C_{3'}$), 70.6 (C_{12}), 65.3 ($C_{11'+11}$), 53.9 ($C_{8'+8}$); pyrrolic ^{13}C $C_{1'}$ and $C_{2'}$ are too enlarged to be observed at 298K. **ES-MS**: m/z (%) calcd for $[C_{128}H_{108}N_{32}O_8Zn]^{2+}/2$: 1142.4154; found : 1142.4172 (100) $[M + 2H^+]/2$.

Synthesis of monometallated cage Zn-L-2H. Zinc acetate $Zn(OAc)_2 \cdot 2H_2O$ (9.85 mg, 44.9 μmol, 1.1 equiv.) was added to a stirred solution of cage ***2H-L-2H*** (97.8 mg, 40.8 μmol, 1 equiv.) in CH_2Cl_2/MeOH (9:1 v/v) and refluxed overnight. The solvents were evaporated and the residue was purified by preparative thin layer chromatography eluted with CH_2Cl_2/$CHCl_3$/MeOH 44/50/10 to afford a purple solid (26.1 mg, 26% yield). **^{1}H NMR** (500 MHz, DMF-d_7): δ (ppm) = 8.52 (8 H, br

s, $H_{pyr'}$), 8.44 (8 H, s, H_{pyr}), 8.29 (4 H, s, H_t), 8.25 (4 H, s, $H_{t'}$), 8.14 (4 H, d, ^3J = 7.6 Hz, $H_{o'\,out}$), 8.09 (4 H, d, ^3J = 7.6 Hz, $H_{o\,out}$), 7.71 (4 H, d, ^3J = 7.6 Hz, $H_{m'\,out}$), 7.66 (4 H, d, ^3J = 7.6 Hz, $H_{m\,out}$), 7.22 (4 H, d, ^3J = 7.6 Hz, $H_{o'\,in}$), 7.17 (4 H, d, ^3J = 7.6 Hz, $H_{o\,in}$), 6.55 (4 H, d, ^3J = 7.6 Hz, $H_{m'\,in}$), 6.52 (4 H, d, ^3J = 7.6 Hz, $H_{m\,in}$), 5.71 (8 H, s, $H_{1'}$), 5.67 (8 H, s, H_1), 4.66 (8 H, s, $H_{2'}$), 4.65 (8 H, s, H_2), 3.71 (16H, m, H_3), 3.66 (16 H, m, H_4), -2.87 (2 H, s, NH). **^{13}C NMR** (126 MHz, DMF-d_7): δ (ppm) = 150.7 (C_2), 146.1 ($C_{10+10'}$), 143.6 (C_4), 142.1 ($C_{4'}$), 136.9 ($C_{5'\,out}$), 136.2 ($C_{5\,out}$), 135.7 ($C_{7'}$), 134.6 ($C_7 + C_{5'\,in+5\,in}$), 132.5 (C_1), 127.5 ($C_{6'\,out}$), 127.1 ($C_{6\,out}$), 126.8 ($C_{6'\,in}$), 126.3 ($C_{6\,in}$), 125.3 ($C_{9'}$), 125.3 (C_9), 121.1 (C_3), 120.8 ($C_{3'}$), 71.4 (C_{12}), 70.7 (C_{13}), 65.2 ($C_{11'+11}$), 53.8 ($C_{8'+8}$); pyrrolic ^{13}C $C_{1'}$ and $C_{2'}$ are too enlarged to be observed at 298K. **ES-MS**: m/z (%) calcd for $[C_{136}H_{122}N_{32}O_{12}ZnNa_2]^{2+}$/2: 1252.4498; found : 1252.4521 (100) [M + 2Na$^+$]/2; calcd for $[C_{136}H_{122}N_{32}O_{12}ZnNa]^+$: 2481.9104 ; found : 2482.9233 (20).

Absorption and emission spectroscopy, photophysics

Spectroscopic grade DCM and MeOH were from Merck and used as received. Silver trifluoromethanesulfonate (Ag(OTf)) was from Sigma–Aldrich and was stored under argon in a sealed vial in dark and dry conditions. Ag(OTf) solutions were used fresh and kept in the dark during the measurements.

Absorption spectra were recorded with Perkin–Elmer Lambda 650 UV-vis and Perkin–Elmer Lambda 950 UV-VIS-NIR spectrophotometers. Integrated absorption coefficients were calculated by plotting molar absorption coefficients as a function of absorption energy (in wavenumbers) and calculating the area under the curves.

Emission spectra were collected with an Edinburgh FLS920 fluorimeter, equipped with a Peltier-cooled Hamamatsu R928 PMT (200–850 nm), and corrected for the wavelength-dependent phototube response. Corrected excitation spectra were recorded with the same fluorimeter. Emission quantum yields were evaluated from the area of the luminescence spectra, corrected for the photomultiplier response, with reference to *meso*-tetraphenylporphyrin in aerated toluene (ϕ_{fl} = 0.11) [41]. Measurements at 77K were performed with the same fluorimeter, making use of Pyrex tubes dipped in liquid nitrogen in a quartz Dewar. Gated emission spectra were acquired by using a time-gated spectral scanning mode and a μF920H Xenon flash lamp (pulse width < 2 μs, repetition rate between 0.1 and 100 Hz) as excitation source. Spectra were corrected for the wavelength-dependent photomultiplier response. Triplet excited state lifetimes were measured with the same apparatus in the multichannel scaling mode.

Fluorescence lifetimes in the nanosecond range were detected by using an IBH Time Correlated Single Photon Counting apparatus with Nano-LED excitation at 465 nm. Analysis of the decay profiles against time was performed using the Decay Analysis Software DAS6 provided by the manufacturer.

Fluorescence lifetimes in the ps regime were measured by means of a Hamamatsu synchroscan streak-camera apparatus (C10910-05 main unit and M10911-01 synchroscan unit) equipped with an ORCA-Flash 4.0 V2 charge-coupled device (CCD) and an Acton spectrograph SP2358. As excitation source, a Newport Spectra Physics Solstice-F-1K-230 V laser system, combined with a TOPAS Prime (TPR-TOPAS-F) optical parametric amplifier (pulse width: 100 fs, 1 kHz repetition rate) [42] was used, tuned at 560 nm. To reduce photo-degradation, the pump energy on the sample was reduced to 26 μJ/pulse. Emission from the sample, collected at a right angle with a 1 mm slit, was focused by means of a system of lenses into the spectrograph slit. Streak images were taken in analog integration mode (100 exposures, exposure time: 2 s). The decays were measured over emission spectral ranges of 20–40 nm. HPD-TA 9.3 software from Hamamatsu was used for data acquisition and analysis. The overall time resolution of the system after deconvolution procedure was 1 ps.

The energy transfer rate in the monometallic cages was calculated as $k_{en} = 1/\tau - 1/\tau_0$, in which τ is the lifetime of the quenched donor unit and τ_0 the lifetime of the unquenched unit, *i.e.* the lifetime of the reference model (the Zn-component in the bis Zn-porphyrin cages): 1.7 ns for **Zn-S-Zn** and 1.6 ns for **Zn-L-Zn** [32]. The error for the energy transfer rate value has been estimated according to the partial derivative methods and by taking the temporal resolution of the measuring system as uncertainty on the lifetime value (1 ps for τ, measured with the streak camera apparatus, and 0.2 ns for τ_0, measured with the Time Correlated Single Photon Counting equipment). The energy transfer efficiency is defined as $\eta_{en} = k_{et}/(k_{et} + \tau_0^{-1})$.

The calculation of the energy-transfer rate constant according to the Förster theory was performed by using equation (1) [43], where d_{DA} is the distance between the centers of mass of the donor and acceptor, Φ and τ_0 are the emission quantum yield and lifetime of the donor, J^F the overlap integral, n the refractive index of the solvent and K^2 the orientation factor, calculated according to equation (2) [44], where θ_D and θ_A are the angles formed between the line connecting the donor and acceptor centers and the transition moments of the donor and acceptor, respectively, and ϕ is the angle between the projections of the transition moments on a plane perpendicular to the line connecting the centers of the donor and the acceptor.

$$k_{en}^F = \frac{8.8\times10^{-25}K^2\Phi}{n^4\tau_0 d_{DA}^6}J^F \qquad (1)$$

$$K^2 = (\sin\theta_D \sin\theta_A \cos\phi - 2\cos\theta_D \cos\theta_A)^2 \qquad (2)$$

Estimated errors are 10% on lifetimes, 20% on quantum yields, 20% on molar absorption coefficients and 3 nm on emission and absorption peaks.

CONCLUSION

The photophysics of flexible covalent cages bearing either two free-base porphyrins or one free-base porphyrin and one Zn(II) porphyrin, connected by flexible linkers of different lengths, has been investigated in detail by means of steady-state and time-resolved spectroscopic studies. Strong exciton interactions between the porphyrins have been evidenced in all cases, due to the close proximity of these units in the collapsed structure of the cages. The emission features of the porphyrins depend on the composition of the cage and/or on the lengths of the linkers: the free-base units display altered fluorescence quantum yield and lifetime only in the monometallated cages, where the Zn counterpart influences their radiative behavior, with a more important reduction in the cage with shorter linkers. The Zn-porphyrins are quantitatively quenched by a fast energy transfer process that sensitizes the free-base emission in both monometallated cages. This photoinduced process is slightly faster in the cage with longer linkers, probably due to the very short interplanar distance between the porphyrins in this cage, supposed to be around 4 Å. The results highlight the role of the linkers and of the arrangement of the components in the photophysics of flexible porphyrinic cages.

Acknowledgments

The International Center for Frontier Research in Chemistry, icFRC (www.icfrc.fr), and the LabEx-CSC are gratefully acknowledged for a Ph.D. fellowship to L.S. The Ministry of Education and Research is acknowledged for a Ph.D. fellowship to R.D. We also thank the ANR Agency for the funding of the project ANR 14-CE06-0010 "Switchable cages" and the Italian CNR (Project "PHEEL"). EC is acknowledged for the NOAH project, grant N. 765297 under H2020-MSCA-ITN-2017. Prof. Isabella Daidone, Dr. Laura Zanetti-Polzi (University of L'Aquila) and Dr. Andrea Barbieri (ISOF-CNR) are thanked for helpful discussion.

Notes

[§] The emission contribution from the model Zn-alkyne in the mixture upon excitation at 630 nm is not negligible at the concentration used, which is optimized for the free-base porphyrin excitation.

REFERENCES

1. Durot S, Taesch J and Heitz V. *Chem. Rev.* 2014; **114**: 8542–8578.
2. Chakrabarty R, Mukherjee PS and Stang PJ. *Chem. Rev.* 2011; **111**: 6810–6918.
3. Mukhopadhyay RD, Kim Y, Koo J and Kim K. *Acc. Chem. Res.* 2018; **51**: 2730–2738.
4. Balaban TS. *Acc. Chem. Res.* 2005; **38**: 612–623.
5. Li W-S, Kim KS, Jiang D-L, Tanaka H, Kawai T, Kwon JH, Kim D and Aida T. *J. Am. Chem. Soc.* 2006; **128**: 10527–10532.
6. Harvey PD, Stern C, Gros CP and Guilard R. *Coord. Chem. Rev.* 2007; **251**: 401–428.
7. Nakamura Y, Aratani N and Osuka A. *Chem. Soc. Rev.* 2007; **36**: 831–845.
8. Satake A and Kobuke Y. *Org. Biomol. Chem.* 2007; **5**: 1679–1691.
9. Gust D, Moore TA and Moore AL. *Acc. Chem. Res.* 2009; **42**: 1890–1898.
10. Wasielewski MR. *Acc. Chem. Res.* 2009; **42**: 1910–1921.
11. Lindsey JS and Bocian DF. *Acc. Chem. Res.* 2011; **44**: 638–650.
12. Pellegrin Y and Odobel F. *Coord. Chem. Rev.* 2011; **255**: 2578–2593.
13. Sprafke JK, Kondratuk DV, Wykes M, Thompson AL, Hoffmann M, Drevinskas R, Chen W-H, Yong CK, Kärnbratt J, Bullock JE, Malfois M, Wasielewski MR, Albinsson B, Herz LM, Zigmantas D, Beljonne D and Anderson HL. *J. Am. Chem. Soc.* 2011; **133**: 17262–17273.
14. Griffith MJ, Sunahara K, Wagner P, Wagner K, Wallace GG, Officer DL, Furube A, Katoh R, Mori S and Mozer AJ. *Chem. Commun.* 2012; **48**: 4145–4162.
15. Wytko JA, Ruppert R, Jeandon C and Weiss J. *Chem. Commun.* 2018; **54**: 1550–1558.
16. Hong S, Rohman MdR, Jia J, Kim Y, Moon D, Kim Y, Ko YH, Lee E and Kim K. *Angew. Chem.* 2015; **127**: 13439–13442.
17. Yu C, Long H, Jin Y and Zhang W. *Org. Lett.* 2016; **18**: 2946–2949.
18. Hwang I-W, Kamada T, Ahn TK, Ko DM, Nakamura T, Tsuda A, Osuka A and Kim D. *J. Am. Chem. Soc.* 2004; **126**: 16187–16198.
19. Hernández-Eguía LP, Escudero-Adán EC, Pintre IC, Ventura B, Flamigni L and Ballester P. *Chem. — Eur. J.* 2011; **17**: 14564–14577.
20. Durot S, Flamigni L, Taesch J, Dang TT, Heitz V and Ventura B. *Chem. — Eur. J.* 2014; **20**: 9979–9990.
21. Huber R. *Angew. Chem., Int. Ed. Engl.* 1989; **28**: 848–869.
22. Deisenhofer J and Michel H. *Angew. Chem., Int. Ed. Engl.* 1989; **28**: 829–847.
23. Deisenhofer J, Epp O, Sinning I and Michel H. *J. Mol. Biol.* 1995; **246**: 429–457.
24. Papiz MZ, Prince SM, Howard T, Cogdell RJ and Isaacs NW. *J. Mol. Biol.* 2003; **326**: 1523–1538.
25. Roszak AW. *Science* 2003; **302**: 1969–1972.
26. Umena Y, Kawakami K, Shen J-R and Kamiya N. *Nature* 2011; **473**: 55–60.
27. Pšenčík J and Tuma R. In The Structural Basis of Biological Energy Generation, Vol **39**, M.F.

Hohmann-Marriot (ed.) Springer Science+Business Media Dodrecht, 2014; pp 77–109.
28. Flamigni L, Ventura B, Oliva AI and Ballester P. *Chem. — Eur. J.* 2008; **14**: 4214–4224.
29. Kocher L, Durot S and Heitz V. *Chem. Commun.* 2015; **51**: 13181–13184.
30. Schoepff L, Kocher L, Durot S and Heitz V. *J. Org. Chem.* 2017; **82**: 5845–5851.
31. Djemili R, Kocher L, Durot S, Peuroren A, Rissanen K and Heitz V. *Chem. — Eur. J.* 2018; **25**: 1 – 8.
32. Zanetti-Polzi L, Amadei A, Djemili R, Durot S, Schoepff L, Heitz V, Ventura B and Daidone I. *J. Phys. Chem. C* 2019; **123**: 13094–13103.
33. Ishihara S, Labuta J, Van Rossom W, Ishikawa D, Minami K, Hill JP and Ariga K. *Phys. Chem. Chem. Phys.* 2014; **16**: 9713–9746.
34. Ding Y, Zhu W-H and Xie Y. *Chem. Rev.* 2017; **117**: 2203–2256.
35. Fransson T, Saue T and Norman P. *J. Chem. Theory Comput.* 2016; **12**: 2324–2334.
36. Minaev B and Ågren H. *Chem. Phys.* 2005; **315**: 215–239.
37. Horiuchi H, Terashima K, Sakai A, Suda D, Yoshihara T, Kobayashi A, Tobita S and Okutsu T. *J. Photochem. Photobiol. Chem.* 2016; **321**: 72–78.
38. Wong KF, Bagchi B and Rossky PJ. *J. Phys. Chem. A* 2004; **108**: 5752–5763.
39. Faure S, Stern C, Guilard R and Harvey PD. *J. Am. Chem. Soc.* 2004; **126**: 1253–1261.
40. Cho HS, Jeong DH, Yoon M-C, Kim YH, Kim Y-R, Kim D, Jeoung SC, Kim SK, Aratani N, Shinmori H and Osuka A. *J. Phys. Chem. A* 2001; **105**: 4200–4210.
41. Seybold PG and Gouterman M. *J. Mol. Spectrosc.* 1969; **31**: 1–13.
42. Briš A, Trošelj P, Margetić D, Flamigni L and Ventura B. *ChemPlusChem* 2016; **81**: 985–994.
43. Főrster Th. *Discuss. Faraday Soc.* 1959; **27**: 7–17.
44. Van Der Meer BW. Coker III G and Simon S-Y Chen. In Resonance Energy Transfer: Theory and Data, Wiley VCH Weinheim, 1994; pp. 55–83.